

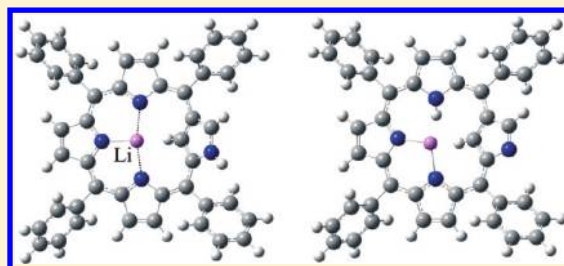
# Computational Insight into the Electronic Structure and Absorption Spectra of Lithium Complexes of N-Confused Tetraphenylporphyrin

Demeter Tzeli,\* Ioannis D. Petsalakis, and Giannoula Theodorakopoulos

Theoretical and Physical Chemistry Institute, National Hellenic Research Foundation, 48 Vassileos Constantinou, Athens 116 35, Greece

**S** Supporting Information

**ABSTRACT:** The present work is a theoretical investigation on lithium complexes of N-confused tetraphenylporphyrins (aka inverted) employing density functional theory (DFT) and time-dependent DFT, using the B3LYP, CAM-B3LYP, and M06-2X functionals in conjunction with the 6-31G(d,p) basis set. The purpose of the present study is to calculate the electronic structure and the bonding of the complexes to explain the unusual coordination environment in which Li is found experimentally and how the Li binding affects the Q and the Soret bands. The calculations show that, unlike a typical tetrahedral  $\text{Li}^+$  cation, this Li forms a typical bond with one N and interacts with the remaining two N atoms, and it is located in the right place to form an agostic-like interaction with the internal C atom. The reaction energy, the enthalpy for the formation of the lithium complexes of N-confused porphyrins, and the effect of solvation are also calculated. The insertion of Li into N-confused porphyrin, in the presence of tetrahydrofuran, is exothermic with a reaction energy calculated to be as high as  $-72.4$  kcal/mol using the lithium bis(trimethylsilyl)amide reagent. Finally, there is agreement in the general shape among the vis-UV spectra determined with different functionals and the experimentally available ones. The calculated geometries are in agreement with crystallographic data, where available.



## I. INTRODUCTION

The N-confused porphyrin (NCP) or inverted porphyrin has attracted the interest of chemists since its first synthesis independently by the Furuta<sup>1</sup> and Latos-Gražynski groups.<sup>2</sup> NCPs are porphyrin isomers having one of the pyrrolic N atoms facing outside of the macrocycle and one C–H group oriented inward toward the core. NCPs have a remarkable ability to bind to a wide variety of cations and anions in their free base and protonated forms, respectively.<sup>3–5</sup> Moreover, they have versatile coordination modes, and they can stabilize some rare high oxidation states of metal ions.<sup>3–6</sup> Additionally, the peripheral nitrogen atom can act as hydrogen bonding donor or acceptor, which is important in the formation of multiporphyrin systems.<sup>4,5</sup> Up to now singly and doubly NCP have been synthesized, i.e., with one and two inverted pyrrole groups.<sup>7</sup> The above properties make NCP a potent candidate for diverse applications in the areas of supramolecular self-assembly and coordination chemistry, in catalysis, in photosynthetic systems, as optical molecular devices, and redox-active materials.<sup>5</sup>

Since the first synthesis of NCP, metal complexes of NCP have been generated using some of the main group elements, lanthanides, and transition metal ions.<sup>3–6,8</sup> While there exist both theoretical and experimental studies on complexes of lithium with normal porphyrins,<sup>9</sup> on lithium NCP there is only one very recent experimental study, of Sripothongnak and Ziegler,<sup>8</sup> where lithium complexes of N-confused tetraphenylporphyrin and its 21-N-methylated variant have been synthesized, characterized by X-ray diffraction and the absorption spectrum of the Li-NCP complex

has been obtained.<sup>8</sup> One of their findings is that Li adopts an unusual coordination environment, unlike that observed in typical tetrahedral  $\text{Li}^+$  cations. This unusual coordination environment was the motivation of the present study. As far as we know, there is no theoretical study on lithium complexes of NCPs, while there are a few computational studies on free-base NCPs.<sup>7,10</sup>

The present work is a theoretical study on lithium complexes of N-confused tetraphenylporphyrins employing density functional theory. One of the objectives is to determine the stability and the binding of the above complexes by geometry optimization calculations of the ground electronic state. Binding of Li to N has been previously studied in diatomic and triatomic systems by one of the authors.<sup>11</sup> Here, we are interested in the binding of the Li with N atoms in Li-NCP, which might lead to the explanation for the unusual behavior of Li as reported experimentally.<sup>8</sup> A further objective is the calculation of excited electronic states and the absorption spectra of the different conformers, as well as the comparison of the calculated absorption spectra with the experimental ones.

## II. COMPUTATIONAL PROCEDURE

We calculated in the gas phase and in toluene solvent the two tautomers of the N-confused tetraphenylporphyrin (**1a** and **1b**), the externally N-methylated N-confused tetraphenylporphyrin (**2**),

**Received:** May 9, 2011

**Revised:** September 7, 2011

**Published:** September 08, 2011

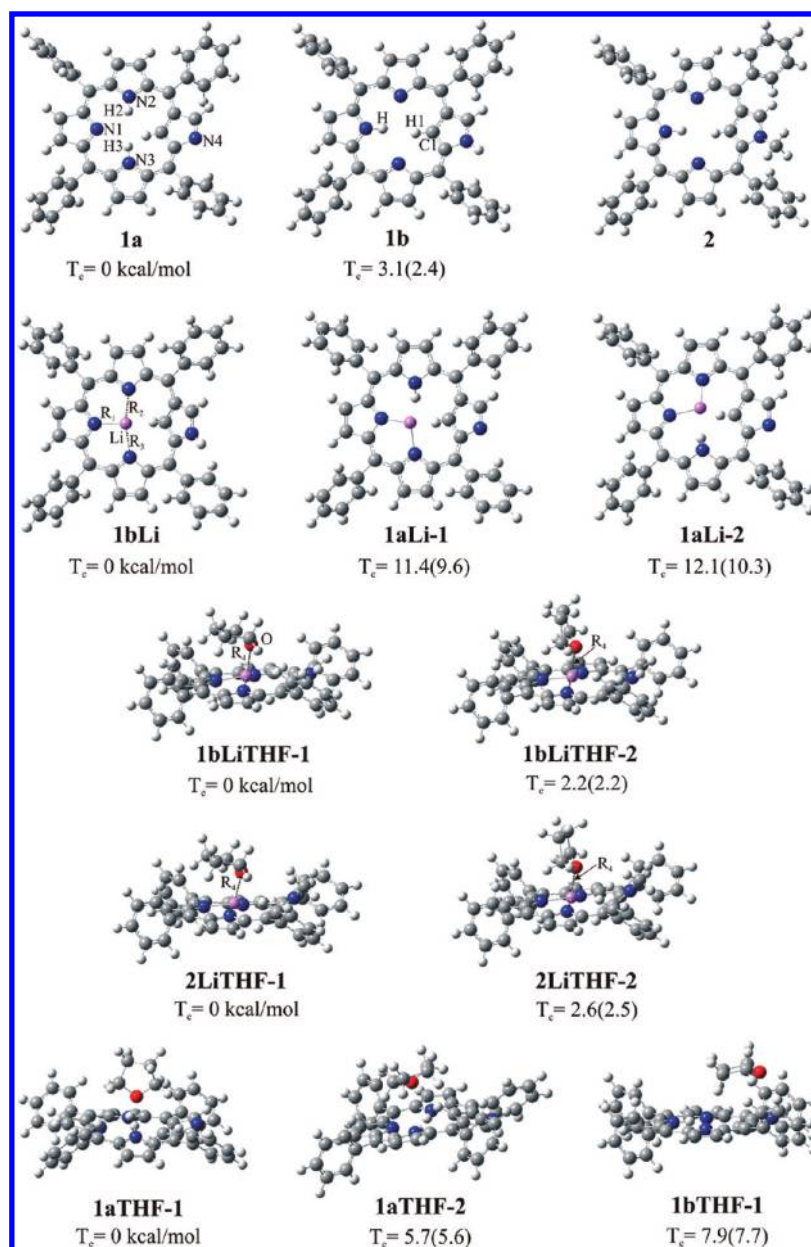


**Figure 1.** 1a, 1b, 2, 1bLi, 1aLi-1, 1aLi-2, 1bLiTHF-1, 1bLiTHF-2, 2LiTHF-1, 2LiTHF-2, 1aTHF-1, 1aTHF-2, and 1bTHF-1 species. Energy differences  $T_e$  from the most stable structure are shown in the gas phase (in toluene solvent) at the M06-2X/6-31G(d,p) level of theory.

the lithium complexes of the 1 NCP (1bLi, 1aLi-1, and 1aLi), and the lithium complexes of the 1 and 2 NCPs in the presence of tetrahydrofuran (THF), (1bLiTHF-1, 1bLiTHF-2, 2LiTHF-1, and 2LiTHF-2); these structures are shown in Figure 1. Moreover, the interaction of the 1 NCP with the THF molecule has been studied. The most stable structures (1aTHF-1, 1aTHF-2, and 1bTHF-1) are given in Figure 1; the remaining ones are given in the Supporting Information. From the above calculated complexes the 1bLi, 1bLiTHF-1, and 2LiTHF-2 structures have been synthesized by the Sripathongnak and Ziegler.<sup>8</sup>

All calculated structures were fully optimized using the B3LYP,<sup>12</sup> CAM-B3LYP,<sup>13</sup> and M06-2X<sup>14</sup> functionals in conjunction with the 6-31G(d,p)<sup>15</sup> basis set in the gas phase and in toluene solvent. B3LYP is a DFT functional using Becke's three-parameter gradient corrected functional with the gradient corrected correlation of Lee, Yang, and Parr.<sup>12</sup> It is a widely used

functional, one of the most often employed in calculations on relevant systems, and it generally works well for the chemistry of main group elements. The CAM-B3LYP<sup>13</sup> functional is a hybrid functional built as B3LYP and includes long-range corrections. M06-2X<sup>14</sup> is a hybrid meta exchange correlation functional and is a highly nonlocal functional with double the amount of nonlocal exchange and is recommended for applications involving main-group elements, kinetics, noncovalent interactions, and electronic excitation energies to valence and Rydberg states.<sup>14</sup> The last functional is expected to be the most appropriate one.

The applicability of the above functionals to the Li–N binding was tested on the diatomic molecule LiN;<sup>11</sup> the Li–N bond distance and the dissociation energy ( $D_e$ ) were compared with very accurate ab initio calculations, i.e., multireference configuration interaction calculations (MRCI/aug-cc-pV5Z<sub>N</sub>/cc-pVQZ<sub>Li</sub>),<sup>11</sup> see Table 1. We observe that the M06-2X/6-31G(d,p) method is in

**Table 1. Bond Distances,  $R_{\text{Li-N}}$  (Å), Dissociation Energies,  $D_e$  (kcal/mol), and Mulliken [NPA] Charges on Li,  $q_{\text{Li}}$  of the  $\text{LiN}(\text{X}^3\Sigma^-)$  Molecule Performing Restricted Open Shell (Unrestricted) Calculations at the B3LYP, CAM-B3LYP, and M06-2X/6-31G(d,p) Levels of Theory**

	$R_{\text{Li-N}}$	$D_e$	$q_{\text{Li}}$
B3LYP	1.878 (1.888)	38.8 (39.3)	0.47[0.72] (0.45[0.70])
CAM-B3LYP	1.864 (1.871)	38.3 (38.7)	0.48[0.74] (0.47[0.73])
M06-2X	1.872 (1.880)	35.4 (35.8)	0.49[0.76] (0.47[0.74])
MRCI <sup>a</sup>	1.879	35.8	0.50

<sup>a</sup> Reference 11, aug-cc-pV5Z<sub>N</sub>/cc-pVQZ<sub>Li</sub>.

complete agreement with the MRCI results for the  $D_e$  values, while the CAM-B3LYP and B3LYP functionals result in small deviations. All three DFT methods are in good agreement with respect to the bond distance of the ab initio method. We also carried out test calculations on the  $\text{Li}(\text{NH}_3)_4^+$  cation, as a typical tetrahedral species of Li, at the M06-2X/6-31G(d,p) level of theory calculating its geometry and both the NPA and the Mulliken population analysis, to compare and contrast this with Li-NCP where Li adopts an unusual coordination environment. The use of both NPA and Mulliken analyses is indicative and helps us to make comparisons and to observe the trends for similar structures when the same basis set is applied; see below in part B of Results and Discussion. Finally, we carried out calculations on lithium bis(trimethylsilyl)amide and bis(trimethylsilyl)amine, i.e.,  $\text{LiN}(\text{Si}(\text{Me})_3)_2$  and  $\text{HN}(\text{Si}(\text{Me})_3)_2$  respectively, at the M06-2X/6-31G(d,p) level of theory, to calculate the reaction energy of the insertion of Li to NCP because the amide is a commonly used reagent for the insertion of lithium in porphyrins.<sup>8</sup> Restricted calculations were carried out for the closed shell systems, while both restricted open shell and unrestricted calculations were performed for the open shell systems.

For all structures shown in Figure 1, the harmonic frequencies were calculated in order to find out which species are true minima. For the inclusion of the toluene solvent, the polarizable continuum model was employed.<sup>16</sup> This model is divided into a solute part lying inside a cavity, surrounded by the solvent part represented as a structureless material characterized by its macroscopic properties, i.e., dielectric constant and solvent radius. This method is one of the most often used and reliable continuum solvation procedures.<sup>17</sup>

The singlet-spin excited electronic states of the separated species and their complexes have been calculated via time-dependent DFT (TDDFT).<sup>18</sup> The lowest 50 excited electronic states of the complexes have been determined at the optimized ground state geometry, relevant to the absorption spectra in order to calculate the Q, B (Soret), N, L, and M bands.<sup>19</sup> The calculations were carried out in the gas phase and in toluene solvent.

For all determined structures, basis set superposition error (BSSE) corrections have been taken into account using the counterpoise procedure<sup>20</sup> since such corrections are important for weak and medium size interactions,<sup>21</sup> which is the case for the structures calculated here. All calculations were performed using the Gaussian 09 program package.<sup>22</sup> The coordinates of all the optimized structures are included in the accompanying Supporting Information.

### III. RESULTS AND DISCUSSION

The two tautomers of the NCP (**1a** and **1b**) and the externally N-methylated N-confused porphyrin (**2**) are shown in Figure 1. The tautomer having three H atoms in the core (**1a**) is more stable than the one having two H atoms (**1b**) by about 3(2) kcal/

mol in the gas phase (toluene solvent) at both the CAM-B3LYP and M06-2X/6-31G(d,p) levels of theory. It has been reported that both tautomers are observed in solution, where **1a** is the preferred tautomer in aromatic and halogenated solvents, while **1b** in highly polar solvents.<sup>1,10,23</sup> The insertion of Li into NCP via the **1b** tautomer results in the **1bLi** structure of Figure 1. The insertion of Li into NCP via the **1a** tautomer yields the **1aLi-1** and **1aLi-2** structures where the H3 and H2 atoms have been replaced by the Li atom, respectively (see Figure 1). As reported in ref 8, in the presence of THF, pseudo-five-coordinate complexes are generated for the lithium complexes of the **1b** and **2** porphyrins. In the present calculations two isomers have been determined for the Li-NCP formed by the **1b** and **2** porphyrins in the presence of THF, labeled as **1bLiTHF-1**, **1bLiTHF-2** and **2LiTHF-1**, **2LiTHF-2**, respectively, in Figure 1; in the -1 isomers the ring of THF is parallel to the core, while in the -2 isomers the THF ring is perpendicular to the core ring. The -1 structures are lower in energy but only by about 2.5 kcal/mol than the corresponding -2 structures, both in the gas phase and in toluene solvent at the M06-2X/6-31G(d,p) level of theory, see Figure 1. All calculated structures in the gas phase are minima with the exception of **2LiTHF-2**, which has one imaginary frequency, obtained by all three functionals. The imaginary frequency (just  $4.2i \text{ cm}^{-1}$  using the B3LYP functional) corresponds to a counter-balanced vibration of the C<sub>2</sub> and C<sub>3</sub> atoms of THF, which does not affect the stability of the complex. It might be noted that experimentally, structure **2LiTHF-2** is reported to be the observed structure in the solid,<sup>8</sup> suggesting that in the solid such a vibration is hindered while there might be some differences in the relative stability between the gas phase and the crystal structures. Finally, calculations on the interaction of the free-base porphyrins **1a** and **1b** with THF obtained the three most stable structures to be the **1aTHF-1** (with the THF ring perpendicular to the core), **1aTHF-2** and **1bTHF-1** structures (with the THF ring parallel to the core) shown in Figure 1.

It is instructive to compare the results of the calculations on the geometries, interaction energies and reaction energies obtained by the three different functionals employed; the B3LYP, the CAM-B3LYP and the more recently designed M06-2X functional. All three functionals predict similar geometries for the same species and in good agreement with the crystallographic data where available. However, the CAM-B3LYP and M06-2X geometries are in closer agreement with experiment than the B3LYP values; see Table 2 and Supporting Information. Furthermore, the B3LYP interaction energies and reaction energies are the smallest values, while the corresponding M06-2X quantities are the largest; see below (Tables 3 and 4). The M06-2X functional may be considered to be more appropriate for the system of interest here since it has been developed to predict noncovalent as well as covalent interactions.<sup>14</sup> Recent studies have shown the M06-2X functional and M06-L (for transition metal energetics)<sup>14</sup> functionals to be more accurate than other functionals for intermolecular interactions using dimers reported in the S22 database.<sup>24</sup> Primarily for this reason and also on the basis of the results of the test calculations on the diatomic LiN discussed above, we consider that the best reaction energies are obtained here with the use of the M06-2X functional. In what follows the results of the calculations will be discussed in detail.

**A. Geometries.** As mentioned above, the optimized geometries are similar using all three functionals, see Supporting Information. Some selected bond lengths obtained using the M06-2X functional are given in Table 2. As already stated the insertion of Li into NCP is

**Table 2. Geometry,  $R$  (Å), and  $\varphi$  (degrees), Mulliken (NPA) Charges of Selected Atoms of the 1a, 1b, 2, 1bLi, 1aLi, 1bLiTHF, 2LiTHF, 1aTHF, and 1bTHF Species in the Gas Phase and in Toluene Solvent at the M06-2X/6-31G(d,p) Level of Theory; Crystallographic Data are also included**

species	$R_{Li-N1}$	$R_{Li-N2}$	$R_{Li-N3}$	$R_{Li-O}$	$R_{Li-C1}$	$R_{Li-H1}$	$R_{Li-HI}$	$\varphi_{HHI-C1}$	$\varphi_H$	$q_{N1}$	$q_{N2}$	$q_{N3}$	$q_{H1}$	$q_{CI}$	$q_O$
<b>1bLi</b>	1.909	2.086	2.059	2.390	1.992	1.078	97.8	0.34(0.63)	-0.68(-0.60)	-0.67(-0.57)	-0.68(-0.59)	0.22(0.27)	-0.22(-0.31)		
<sup>a</sup>	1.916	2.093	2.067	2.394	2.005	1.079	97.3	0.34(0.64)	-0.68(-0.61)	-0.67(-0.57)	-0.68(-0.59)	0.22(0.27)	-0.22(-0.31)		
<sup>b</sup>	1.916(6)	2.067(6)	2.085(6)	2.363(6)	1.981	1.005	99.4(3)								
<b>1aLi-1</b>	1.979	2.614	1.927	2.398	2.078	1.083	93.3	0.38(0.73)	-0.72(-0.64)	-0.72(-0.61)	-0.69(-0.61)	0.18(0.24)	-0.24(-0.38)		
<b>1aLi-2</b>	1.980	1.926	2.616	2.379	2.057	1.083	93.3	0.38(0.73)	-0.72(-0.64)	-0.69(-0.61)	-0.72(-0.60)	0.18(0.23)	-0.23(-0.39)		
<b>1bLiTHF-1</b>	1.942	2.125	2.131	1.987	2.395	2.048	94.9	0.28(0.55)	-0.62(-0.60)	-0.63(-0.54)	-0.64(-0.57)	0.24(0.28)	-0.21(-0.29)		-0.52(-0.59)
<sup>a</sup>	1.942	2.127	2.134	1.985	2.396	2.044	95.2	0.28(0.55)	-0.62(-0.60)	-0.63(-0.55)	-0.64(-0.57)	0.24(0.28)	-0.21(-0.29)		-0.53(-0.59)
<sup>b</sup>	1.938(4)	2.149(4)	2.156(4)	1.983(4)	2.482(4)	2.040	106.0(2)								
<b>1bLiTHF-2</b>	1.943	2.116	2.120	1.983	2.398	2.029	96.2	0.27(0.55)	-0.63(-0.59)	-0.63(-0.55)	-0.64(-0.56)	0.24(0.28)	-0.21(-0.29)		-0.53(-0.59)
<b>2LiTHF-1</b>	1.943	2.125	2.113	2.004	2.406	2.149	90.1	0.30(0.56)	-0.62(-0.60)	-0.62(-0.54)	-0.64(-0.58)	0.22(0.28)	-0.23(-0.29)		-0.52(-0.59)
<sup>a</sup>	1.946	2.130	2.113	2.002	2.407	2.138	90.7	0.29(0.56)	-0.62(-0.61)	-0.62(-0.54)	-0.64(-0.58)	0.22(0.28)	-0.23(-0.29)		-0.52(-0.59)
<b>2LiTHF-2</b>	1.949	2.120	2.101	1.992	2.405	2.131	90.3	0.28(0.56)	-0.63(-0.60)	-0.63(-0.55)	-0.64(-0.57)	0.22(0.28)	-0.23(-0.29)		-0.53(0.60)
<sup>b</sup>	1.969(6)	2.172(7)	2.156(7)	2.036(7)	2.416(6)	2.108	0.929								

species	$R_{H-N1}$	$R_{H2-O}$	$R_{H3-O}$	$R_{H1-O}$	$R_{Cl-H1}$	$R_{Cl-HI}$	$\varphi_{HHI-C1}$	$\varphi_H$	$q_{N1}$	$q_{N2}$	$q_{N3}$	$q_{H1}$	$q_{CI}$	$q_O$
<b>1aTHF-1</b>		2.063	2.024		1.081			-0.65(-0.58)	-0.69(-0.56)	-0.67(-0.55)	0.15(0.26)	-0.16(-0.30)		-0.56(-0.63)
<b>1aTHF-2</b>				2.184	1.082			-0.69(-0.60)	-0.67(-0.56)	-0.68(-0.53)	0.14(0.25)	-0.17(-0.34)		-0.51(-0.59)
<b>1a</b>					1.081			-0.72(-0.61)	-0.70(-0.56)	-0.69(-0.55)	0.14(0.25)	-0.19(-0.33)		
<b>1b</b>	1.016				1.073	139.6	0.34(0.50)	-0.70(-0.58)	-0.64(-0.54)	-0.65(-0.55)	0.16(0.29)	-0.07(-0.22)		
<b>2</b>	1.017				1.075	130.0	0.34(0.50)	-0.71(-0.58)	-0.64(-0.53)	-0.64(-0.54)	0.15(0.29)	-0.08(-0.22)		

<sup>a</sup> In toluene solvent. <sup>b</sup> Reference 8, crystallographic data.

**Table 3.** BSSE Corrected Interaction Energies in kcal/mol of the **1a**, **1b**, and **1bLi** NCPs with the THF Molecule in the Gas Phase (in Toluene Solvent) at the B3LYP, CAM-B3LYP, and M06-2X/6-31g(d,p) Levels of Theory

	1aTHF-1	1aTHF-2	1bTHF-1	1bLiTHF-1	1bLiTHF-2
B3LYP	-4.8 (-4.0)	-2.8 (-2.2)	-3.8 (-3.6)	-7.5 (-5.9)	-7.3 (-6.2)
CAM-B3LYP	-7.0 (-6.2)	-4.1 (-3.5)	-5.0 (-3.7)	-9.8 (-8.2)	-9.3 (-8.0)
M06-2X	-16.2 (-15.4)	-11.0 (-10.1)	-11.9 (-10.5)	-19.3 (-17.6)	-17.5 (-15.8)

**Table 4.** Reaction Energies,  $\Delta E^a$  (kcal/mol), Enthalpies  $\Delta H^{a,b}$  (kcal/mol), and Gibbs Free Energies  $\Delta G^{a,b}$  (kcal/mol) for the Formation of the **1bLi**, **1aLi**, **1bLiTHF**, **2LiTHF** Species for Different Reactions in the Gas Phase (in Toluene Solvent) at the B3LYP, CAM-B3LYP, and M06-2X/6-31g(d,p) Levels of Theory

	1bLi <sup>c</sup>	1aLi-1	1aLi-2	1bLiTHF-1 <sup>c</sup>	1bLiTHF-2 <sup>c</sup>	2LiTHF-1	2LiTHF-2	
NCP + LiN(Si(Me) <sub>3</sub> ) <sub>2</sub> → Li-NCP + HN(Si(Me) <sub>3</sub> ) <sub>2</sub> or NCP + LiN(Si(Me) <sub>3</sub> ) <sub>2</sub> + THF → Li-NCP-THF + HN(Si(Me) <sub>3</sub> ) <sub>2</sub>								
M06-2X	$\Delta E$	-47.7(-37.3)	-37.2(-28.5)	-36.4(-27.8)	-67.6(-55.4)	-65.7(-53.6)	-72.4(-59.3)	-70.3(-57.2)
	$\Delta H$	-48.1(-37.6)	-37.4(-28.7)	-36.5(-27.8)	-65.2(-54.1)	-63.1(-52.0)	-70.2(-58.1)	-68.5(-56.5)
	$\Delta G$	-47.6(-37.1)	-36.2(-27.5)	-35.1(-26.5)	-53.6(-42.5)	-52.3(-41.2)	-58.2(-46.1)	-55.5(-43.5)
NCP + Li → Li-NCP + H or NCP + Li + THF → Li-NCP-THF + H <sup>d</sup>								
B3LYP	$\Delta E$	-11.3(-7.0)	-0.8(1.9)	0.1(2.7)	-19.1(-13.2)	-18.9(-13.5)	-25.4(-18.8)	-24.9(-18.4)
CAM-B3LYP	$\Delta E$	-14.4(-10.0)	-2.3(0.4)	-1.6(1.2)	-24.5(-18.5)	-24.0(-18.3)	-28.5(-21.7)	-28.1(-21.4)
M06-2X	$\Delta E$	-18.6(-14.6)	-7.7(-5.5)	-7.0(-4.7)	-38.1(-32.4)	-36.3(-30.6)	-42.9(-36.3)	-40.8(-34.2)
	$\Delta H$	-24.3(-20.3)	-13.6(-11.4)	-12.7(-10.5)	-41.5(-36.8)	-39.4(-34.7)	-46.5(-40.8)	-44.7(-39.1)
	$\Delta G$	-23.6(-19.5)	-12.2(-10.0)	-11.1(-8.9)	-29.6(-24.9)	-28.3(-23.6)	-34.2(-28.5)	-31.5(-25.9)
NCP + Li <sup>+</sup> → Li-NCP + H <sup>+</sup> or NCP + Li <sup>+</sup> + THF → Li-NCP-THF + H <sup>+</sup>								
M06-2X	$\Delta E$	168.7(178.0)	179.2(186.7)	179.9(187.5)	148.8(159.8)	150.6(161.6)	144.0(155.9)	146.1(158.0)
	$\Delta H$	162.6(171.9)	173.3(180.8)	174.2(181.7)	145.5(155.4)	147.5(157.5)	140.5(151.4)	142.2(153.0)
	$\Delta G$	163.3(172.6)	174.7(182.2)	175.8(183.3)	157.3(167.2)	158.6(168.6)	152.7(163.6)	155.4(166.3)

<sup>a</sup> BSSE-corrected values. <sup>b</sup> At 1 atm and 298.15 K. <sup>c</sup> The  $\Delta E$ ,  $\Delta H$ , and  $\Delta G$  values have been calculated with respect to the most stable **1a** isomer of the NCP. <sup>d</sup> The restricted open shell and the unrestricted calculations result in the same  $\Delta E$ ,  $\Delta H$ , and  $\Delta G$  values.

favoured via the **1b** tautomer. The lithium atom replaces the H of N1 and also interacts with the other two inner N2 and N3 atoms; see Figure 1. The insertion of Li into tautomer **1a** of the NCP results in **1aLi-1** or **1aLi-2**, which are practically degenerate and less stable than **1bLi** by  $\sim 11$  kcal/mol; see Figure 1. In the **1bLi** structure, the  $R_{\text{Li-N1}}$  bond distance is calculated to be shorter than the  $R_{\text{Li-N2}}$  and  $R_{\text{Li-N3}}$  by 0.2 Å, using all three functionals. The  $R_{\text{Li-N1}}$  distance is 1.909(1.916) Å in **1bLi** in the gas phase (in toluene solvent). The corresponding crystallographic data give a distance of 1.916(6) Å.<sup>8</sup> It might be noted that the calculated  $R_{\text{Li-N1}}$  distance is very close to the bond length calculated for the diatomic LiN (1.880 Å of Table 1) in the ground electronic state,  $X^3\Sigma^-$ , where a single bond of  $\sigma$  character is formed.<sup>11</sup> The  $R_{\text{Li-N2}}$  and  $R_{\text{Li-N3}}$  bond distances in **1bLi** are 2.086 and 2.059 Å, which are very similar to our  $R_{\text{Li-N}}$  bond distances of 2.068 Å in the  $\text{Li}(\text{NH}_3)_4^+$  cation, i.e., the tetrahedral  $\text{Li}^+$  cation with four  $\text{NH}_3$  molecules. In the  $\text{Li}(\text{NH}_3)_4^+$  cation, the Li-N interaction is through the lone pair of the ammonia ligands. All the above indicate that the Li-N1 bond is a single bond, while the Li-N2 and Li-N3 bonds are dative interactions of the negatively charged N2 and N3 atoms with the Li atom, which is positively charged (see below).

The **1aLi-1** or **1aLi-2** structures present a Li-N bond distance of 1.93 Å and a Li-N bond distance of 1.98 Å. The shortest bond distance corresponds to the H-N bond whose H has been removed upon lithium insertion. The Li-N bond distance of Li with the protonated N atom is 2.61 Å. In these two structures the Li atom forms dihedral angles with the three N atoms,  $d_{\text{N2N1N3Li}} = 32.9$  and  $22.9^\circ$ , respectively, while in the **1bLi** structure the

corresponding angle is only  $9.9^\circ$ . Moreover, the displacement of the Li atom from the plane of the three inner N atoms is  $\sim 0.25$  Å in **1bLi** and  $\sim 0.45$  Å in **1bLiTHF** and **2LiTHF** structures, while it is as large as  $\sim 0.8$  Å in the **1aLi-1** and **1aLi-2** structures both in the gas phase and in solvent. As mentioned above, the **1aLi-1** and **1aLi-2** structures have not been synthesized and are calculated here to be less stable than **1bLi** structure by about 11 kcal/mol.

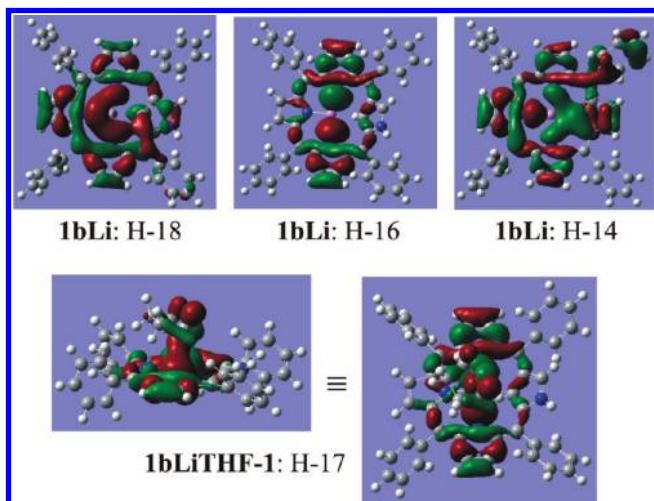
The presence of the THF results in elongations of the  $R_{\text{Li-N}}$  bonds. The lithium complexes of **1b** and **2** with THF have a  $R_{\text{Li-N1}}$  distance elongated by 0.03 Å, while the other two  $R_{\text{Li-N2}}$  and  $R_{\text{Li-N3}}$  bond distances are elongated by up to 0.07 Å with respect to the corresponding complexes without THF. Similar elongations are observed in the crystallographic data of the two lithium complexes of porphyrin **1bLiTHF** and **2LiTHF** products.<sup>8</sup> In all lithium complexes with or without THF, the calculated  $R_{\text{Li-C1}}$  and  $R_{\text{Li-H1}}$  distances range from 2.38 to 2.41 Å and from 1.99 to 2.15 Å, respectively, at the M06-2X/6-31G(d,p) level of theory, while the  $\phi_{\text{LiH1C1}}$  angle ranges from  $90$  to  $98^\circ$ . The  $R_{\text{C1-H1}}$  bond distance in the lithium complexes is slightly elongated with respect to the free base NCP. The above distances and angles are typical for agostic bonds; however, we do not have a transition metal; thus the interaction of Li with C-H can be characterized as an agostic-like interaction.

In the **1aTHF-1** structure, the **1a** tautomer interacts with THF through O-H2 and O-H3 bonds with bond distances of 2.063 and 2.024 Å, while in the **1aTHF-2** structure, the **1a** tautomer interacts with THF mainly through the O-H1 bond whose bond

distance is 2.184 Å at the M06-2X/6-31G(d,p) level of theory. In the **1b**THF-1 structure, the **1b** tautomer binds with THF through interactions of the H atoms of THF with the N atoms of the macrocycle of porphyrin. Finally, the geometry of calculated structures in toluene solvent is very similar to the corresponding geometry in the gas phase, see Table 2.

**B. Bonding.** The Mulliken and the natural population (NPA) analysis of selected atoms of the calculated structures are given in Table 2. It is well-known that Mulliken charges can show basis set dependency<sup>25</sup> or underestimation of the ionic character. The NPA method is considered as an improved alternative to the extensively used Mulliken population, but NPA can also present some problems<sup>26</sup> or can overestimate the ionic character of the atoms.<sup>27</sup> However, it is generally agreed that the use of both population analyses is indicative and helps us to make comparisons for similar structures. All three functionals predict practically the same charges on the atoms within the same type of analysis. While in both Mulliken and NPA the internal N atoms have negative charges of about  $-0.6 e^-$  in all cases; the Li atom has a positive charge that depends on the population analysis used, i.e., about  $+0.3 e^-$  (Mulliken) and about  $+0.6 e^-$  (NPA). We can assume that the charge on Li is about  $0.5 e^-$ . It is worth noting that the **1aLi-1** and **1aLi-2** isomers, which are higher in energy than **1bLi**, present larger charges than the remaining structures using both Mulliken and NPA. In these two structures the Li atoms are further away from the N planes as mentioned above. Finally, using both population analyses the H1 and C1 atoms involved in the agostic-like bond have similar charges of about  $+0.25$  and  $-0.25 e^-$  and the O atom of THF has about  $-0.55 e^-$ .

From the geometries of the **1bLi**, **1bLiTHF**, and **2LiTHF** structures, their molecular orbitals (MOs), population charges, and the comparison with the corresponding values of the LiN and Li(NH<sub>3</sub>)<sub>4</sub><sup>+</sup> species, we conclude that the Li atom in the **1bLi**, **1bLiTHF**, and **2LiTHF** structures is in its ground  $^2S(1s^2 2s^1)$  state. It might be noted that these systems have highly delocalized orbitals, and the natural bond orbital analysis presents problems for some orbitals. For example, there are very low-lying occupied orbitals with occupation number 1.6 and some other occupied orbitals with 1.1  $e^-$  instead of 2. Thus, the canonical MOs which represent the bonding of Li are presented below.



We conclude that a  $\sigma$  bond (Li–N1) is formed between the singly occupied  $p_z$  orbital of N1 and the  $2s$  of Li with partial  $p_z$  mixing. The Li–N2 and Li–N3 bonds involve interactions with

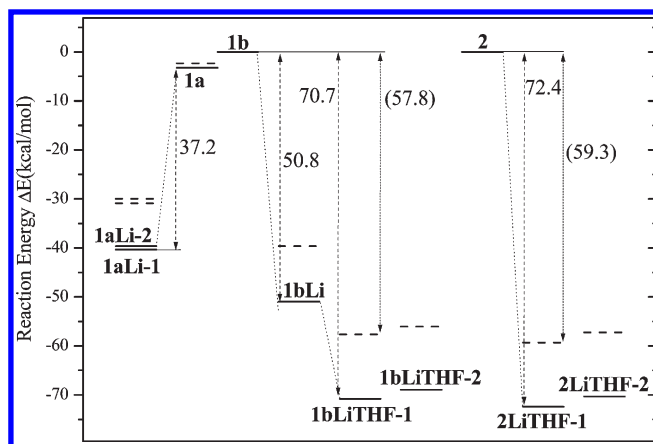
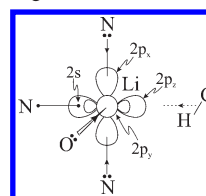
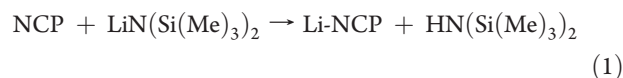


**Figure 2.** Reaction energies for the insertion of lithium in **1a**, **1b**, and **2** NCPs via the reaction  $\text{NCP} + \text{LiN}(\text{Si}(\text{Me})_3)_2 \rightarrow \text{Li-NCP} + \text{HN}(\text{Si}(\text{Me})_3)_2$  in the gas phase (solid line) and in toluene solvent (dotted line) at the M06-2X/6-31G(d,p) level of theory.

the empty  $p_x$  orbital of Li; see the H-16 orbital of **1bLi** in icon above. In the presence of THF, the O atom of the THF molecule interacts with the empty  $p_y$  orbital of the Li atom; see the H-17 orbital of **1bLiTHF-1** given under two different viewing angles. All Li bonding interactions are shown pictorially in the following valence-bond Lewis diagram<sup>11</sup>



**C. Energetics.** The reaction energy for the insertion of lithium into **1a**, **1b**, and **2** NCPs has been calculated for the reaction



LiN(Si(Me)<sub>3</sub>)<sub>2</sub> is the reagent used in the experiment.<sup>8</sup> The M06-2X reaction energy (at absolute zero) of reaction 1 is  $-47.7(-37.3)$  kcal/mol for the production of the **1bLi** NCP with respect to the energy lowest **1a** tautomer in the gas phase (in toluene solvent) or  $-50.8(-39.7)$  kcal/mol with respect to the **1b** tautomer; see Figure 2 and Table 4. In the presence of THF, the reaction energies for the formation of the lowest-energy isomers, cf., **1bLiTHF** and **2LiTHF**, are  $-67.6(-55.4)$  and  $-72.4(-59.3)$  kcal/mol, respectively. Finally, the enthalpies of reaction 1 in the gas phase (in toluene solvent) at 1 atm and 298.15 K for the formation of the **1bLi**, **1bLiTHF** and **2LiTHF** structures are  $-48.1(-37.6)$ ,  $-65.2(-54.1)$ , and  $-70.2(-58.1)$  kcal/mol, respectively, see Table 4.

Reaction 1 is probably a multistep reaction. One possible way is the homolytic cleavage of the Li–N bond of the LiN(Si(Me)<sub>3</sub>)<sub>2</sub> molecule, then the substitution of the H atoms attached to the internal N atoms of NCP with the Li atom and finally the formation of the HN(Si(Me)<sub>3</sub>)<sub>2</sub> molecule, reactions 2, 3, and 4, respectively.



**Table 5. Reaction Energies  $\Delta E^a$  (kcal/mol), Enthalpies  $\Delta H^{a,b}$  (kcal/mol), and Gibbs Free Energies  $\Delta G^{a,b}$  (kcal/mol) for the Reactions 2, 4, 5, and 7 in the Gas Phase (in Toluene Solvent) at the M06-2X/6-31g(d,p) Level of Theory**

reaction <sup>c</sup>	2 <sup>d</sup>	4 <sup>d</sup>	5	6
$\Delta E$	87.3(92.3)	-114.8(-114.5)	158.7(72.6)	-373.3(-287.1)
$\Delta H$	86.7(92.9)	-108.6(-108.3)	157.7(72.2)	-366.5(-279.8)
$\Delta G$	77.3(81.5)	-99.5(-99.1)	148.5(84.2)	-357.6(-274.1)

<sup>a</sup> BSSE-corrected values. <sup>b</sup> At 1 atm and 298.15 K. <sup>c</sup> (2)  $\text{LiN}(\text{Si}(\text{Me})_3)_2 \rightarrow \text{Li}^+ + \text{N}(\text{Si}(\text{Me})_3)_2$ ; (4)  $\text{H}^+ + \text{N}(\text{Si}(\text{Me})_3)_2 \rightarrow \text{HN}(\text{Si}(\text{Me})_3)_2$ ; (5)  $\text{LiN}(\text{Si}(\text{Me})_3)_2 \rightarrow \text{Li}^+ + \text{N}(\text{Si}(\text{Me})_3)_2$ ; (6)  $\text{H}^+ + \text{N}(\text{Si}(\text{Me})_3)_2 \rightarrow \text{HN}(\text{Si}(\text{Me})_3)_2$ . <sup>d</sup> Restricted open shell calculations. The unrestricted calculations result in  $\Delta E$ ,  $\Delta G$ , and  $\Delta H$  values smaller by  $\sim 0.7$  kcal/mol than the restricted ones.

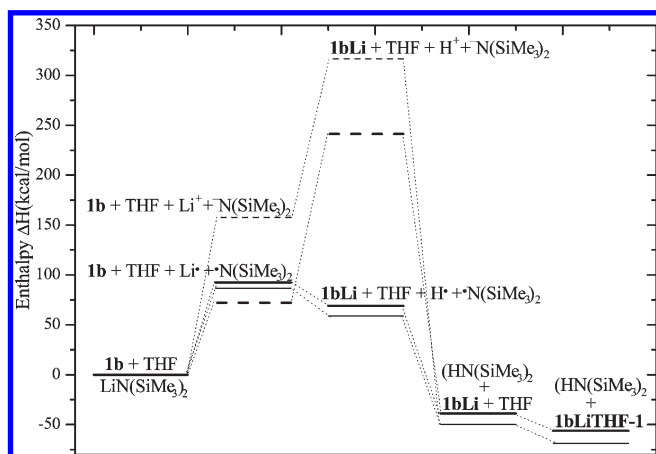
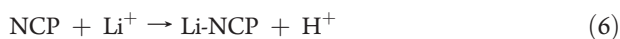
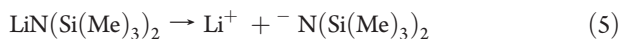


**Figure 3.** Enthalpies for the insertion of lithium in **1b** via the reaction  $\text{1b} + \text{LiN}(\text{Si}(\text{Me})_3)_2 + \text{THF} \rightarrow \text{1bLiTHF-1} + \text{HN}(\text{Si}(\text{Me})_3)_2$  in the gas phase (thin lines) and in toluene solvent (wide line) via the atom exchange (solid lines) or the ion exchange (dashed lines) at the M06-2X/6-31G(d,p) level of theory, at 1 atm and 298.15 K.

Another possible way is the heterolytic cleavage of the Li–N bond of the  $\text{LiN}(\text{Si}(\text{Me})_3)_2$  molecule, then the substitution of the  $\text{H}^+$  cation attached to the internal N atom of NCP with the  $\text{Li}^+$  cation, and finally the formation of the  $\text{HN}(\text{Si}(\text{Me})_3)_2$  molecule, reactions 5, 6, and 7, respectively.



The reaction energies, the enthalpies, and the Gibbs free energies of the above reactions are given in Tables 4 and 5. The relative enthalpies of these two possible routes are depicted in Figure 3. It seems that the first route is more likely to occur, and the atom rather than the ion is exchanged. Note the substantial stabilization of the ions due to the solvent.

The calculated interaction energies of the **1a**, **1b**, and **1bLi** NCPs with THF range from  $-11.0$  to  $-19.3$  kcal/mol and from  $-10.1$  to  $-17.6$  kcal/mol in the gas phase and in toluene solvent, respectively, see Table 3. The largest value corresponds to the **1bLi** NCP, where there is an O–Li interaction. In **1aTHF-1**, the

**1a** tautomer interacts with THF through the O–H2 and O–H3 bonds resulting in an interaction energy of  $-16.2$  ( $-15.4$ ) kcal/mol. The B3LYP reactions energies are about half of M06-2X, while the CAM-B3LYP is between the B3LYP and M06-2X values. However, as discussed above the M06-2X values are expected to be the most accurate ones.<sup>24</sup>

**D. Absorption Spectra.** Excitation energies ( $\Delta E$ ), major peaks ( $\lambda$ ), oscillator strengths ( $f$ -value), main excitations, and their coefficient contributing to the excited state of calculated structures for the lowest-energy Q and Soret bands, calculated via TDDFT, are given in Table 6 and in Tables 2S and 3S of the Supporting Information. The corresponding calculated absorption spectra in the gas phase and in toluene solvent are depicted in Figure 4 and in Figures 1S–6S of the Supporting Information. As can be seen from the above Tables and Figures and from our previous studies on the absorption spectra of complexes of  $\text{C}_{60}$  and  $\text{C}_{59}\text{N}$  and supramolecular complexes of fullerene crown ethers with exTTF and its derivatives,<sup>28,29</sup> different functionals lead to some differences in the calculated  $\lambda_{\text{max}}$  values (absorption maxima), while there is agreement in the general shape of the vis–UV spectra obtained with the different functionals. As we found in the present study the CAM-B3LYP and M06-2X absorption peaks are similar, while the corresponding B3LYP peaks are shifted to smaller energies. The types of excitations corresponding to the excited states are the same in all three functionals. In this section, we test the suitability of the above functionals for the calculation of the absorption spectra using the experimental ones as a guide.

By use of all three functionals, for the **1a** species and all complexes, which include the **1a** NCP, i.e., **1aLi-1**, **1aLi-2**, **1aTHF-1**, and **1aTHF-2**, in their Q-band region there are two peaks with similar oscillator strengths. On the contrary, in all species which include the **1b** or **2** porphyrins, the second Q peak in their absorption spectra has a smaller oscillator strength than the first one, i.e., the lowest-energy Q peak. The general shape of the vis–UV spectra is the same for all complexes containing the **1a** NCP. The same stands for all structures containing the **1b** and **2** NCP. Our results on **1a** and **1b** are in agreement with the results of Vyas et al.<sup>10</sup> who calculated the absorption spectra of the two isomers at the TD-B3LYP/6-31+G(d)//B3LYP/6-31G(d) level of theory, in the gas phase and in  $\text{CH}_2\text{Cl}_2$  (for **1a**) and in  $\text{CH}_3\text{CN}$  (for **1b**) solvents.

In all structures the symmetry is  $C_1$  rather than  $D_{4h}$ , hence the two highest-occupied molecular orbitals (HOMOs, H-1 and H) as well as the two lowest-unoccupied molecular orbitals (LUMOs, L and L+1) are not degenerate. However, excitations among these four orbitals result in the transitions of the Q and Soret (B) bands as in the case of the normal porphyrin derivatives in the four-electron four-orbital model.<sup>33,34</sup> The M06-2X electron density plots of the frontier orbitals of the **1a**, **1b**, **1bLi**, **1aLi-1**, and **2LiTHF-1** species are depicted in Figure 5. The **1b**, **1bLi**, **1bLiTHF**, and **2LiTHF** structures have the same H-1, H, L, and L+1 orbitals. Likewise, the **1a** and **1aLi** have the same frontier orbitals. The replacement of the H by the Li atom, or the interaction of the THF molecule with the Li atom of the Li-NCP isomers, does not change the general shape of these orbitals, but it influences the energy differences of the orbitals; see Table 4S of the Supporting Information. The lowest-energy Q peak corresponds mainly to an excitation from the H orbital to the L, see Table 6. The major peak of the Soret band corresponds to excitation from the H-1 to the L orbital (having the largest coefficient) and from the H to the L+1 orbital.

**Table 6.** Excitation Energies,  $\Delta E_e$  (eV), Absorption Selected Peaks (Lowest-Energy Q and Major Soret Peaks),  $\lambda$  (nm), Oscillator Strengths,  $f$ , Main Excitations, and their Coefficient Contributing to the Excited State of 1a, 1b, 2, 1bLi, 1bLiTHF, 2LiTHF, and 1aTHF Species in the Gas Phase and in Toluene Solvent at the B3LYP, CAM-B3LYP, and M06-2X/6-31G(d,p) Levels of Theory

	B3LYP <sup>b</sup>			CAM-B3LYP <sup>b</sup>			M06-2X <sup>b</sup>			B3LYP <sup>c</sup>			CAM-B3LYP <sup>c</sup>			M06-2X <sup>c</sup>		
	$\Delta E_e$	$\lambda$	$f$	$\Delta E_e$	$\lambda$	$f$	$\Delta E_e$	$\lambda$	$f$	$\Delta E_e$	$\lambda$	$f$	$\Delta E_e$	$\lambda$	$f$	$\Delta E_e$	$\lambda$	$f$
1a	1.95	636	0.075	1.96	632	0.049	2.01	617	0.060	1.93	644	0.13	1.94	639	0.085	1.99	624	0.11
	3.12	397	1.03	3.32	373	1.33	3.30	375	1.32	2.97	417	1.45	3.14	394	1.63	3.13	396	1.59
1b	1.78	696	0.17	2.07	600	0.17	2.06	603	0.19	1.76	703	0.24	2.05	606	0.23	2.03	609	0.26
	3.06	405	0.76	3.37	368	1.35	3.32	373	1.35	2.90	427	1.46	3.20	388	1.72	3.15	393	1.75
2	1.77	700	0.17	2.07	600	0.17	2.05	606	0.19	1.75	707	0.24	2.05	606	0.23	2.03	612	0.26
	3.00	413	0.62	3.33	372	1.32	3.28	377	1.37	2.87	432	1.49	3.17	391	1.68	3.12	397	1.72
1bLi	1.70	729	0.21	1.86	667	0.23	1.87	664	0.25	1.67	744	0.29	1.82	681	0.31	1.83	679	0.34
	2.97	417	0.86	3.28	378	1.37	3.24	382	1.42	2.83	438	1.56	3.11	399	1.73	3.04	404	1.75
1bLiTHF-1	1.65	754	0.19	1.80	688	0.21	1.82	681	0.23	1.62	765	0.27	1.77	699	0.28	1.79	692	0.31
	2.93	422	0.70	3.22	385	1.22	3.19	389	1.26	2.81	442	1.43	3.08	402	1.57	3.05	407	1.59
1bLiTHF-2	1.64	754	0.19	1.80	689	0.21	1.83	679	0.23	1.62	767	0.27	1.77	701	0.29	1.80	690	0.31
	2.94	422	0.70	3.23	384	1.24	3.20	388	1.28	2.81	442	1.43	3.08	402	1.59	3.05	406	1.62
2LiTHF-1	1.63	761	0.19	1.80	689	0.21	1.81	685	0.23	1.60	773	0.26	1.77	700	0.28	1.78	696	0.31
	2.89	429	0.56	3.20	387	1.22	3.16	393	1.23	2.78	445	1.42	3.06	405	1.56	3.02	410	1.56
2LiTHF-2	1.63	762	0.19	1.80	690	0.21	1.82	682	0.23	1.60	774	0.26	1.77	702	0.29	1.78	695	0.31
	2.89	429	0.57	3.20	387	1.22	3.16	392	1.25	2.78	445	1.42	3.06	405	1.57	3.02	410	1.59
1aTHF-1	1.83	678	0.10	1.91	650	0.080	1.90	653	0.088	1.80	689	0.17	1.87	662	0.13	1.87	663	0.14
	3.04	407	0.97	3.25	382	1.13	3.22	385	1.12	2.92	425	1.29	3.10	400	1.42	3.03	403	1.38
1aTHF-2	1.94	640	0.074	1.96	632	0.048	2.00	620	0.057	1.91	648	0.13	1.94	640	0.082	1.99	624	0.10
	3.10	400	0.98	3.29	377	1.21	3.28	378	1.19	2.96	418	1.36	3.14	395	1.52	3.13	397	1.47

<sup>a</sup> Excited state. <sup>b</sup> In the gas phase. <sup>c</sup> In toluene solvent.

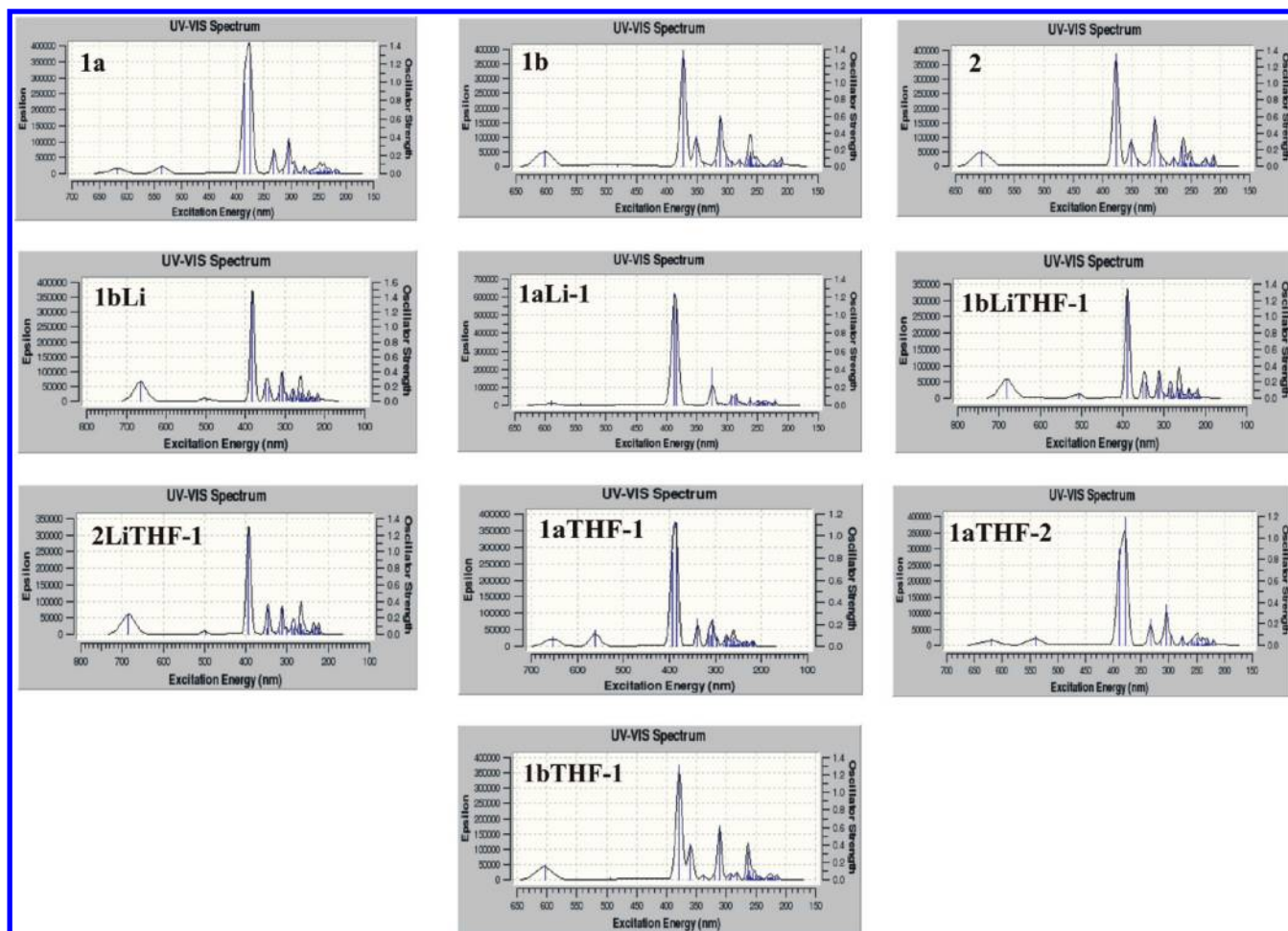


**Figure 4.** Absorption spectrum (molar absorptivity,  $\epsilon$  vs excitation energy) of **1a**, **1b**, **2**, **1bLi**, **1aLi**, **1bLiTHF-1**, **2LiTHF-1**, **1aTHF-1**, and **1bTHF-1** species in the gas phase calculated at the TD-M06-2X/6-31G(d,p) level of theory. The absorption spectra of all calculated species in the gas phase and in toluene at the TD-B3LYP, TD-CAM-B3LYP, and TD-M06-2X/6-31G(d,p) levels of theory are given in the Supporting Information.

**1a NCPs.** For the lowest-energy Q peak of the **1a** tautomer, in the gas phase, all three functionals predict similar wavelength, i.e., it ranges from 617 to 636 nm, see Table 6. The peak is red-shifted when the **1a** tautomer interacts with a THF molecule, i.e., in the **1aTHF-1** structure, and the peak ranges from 650 to 678 nm using different functionals. In toluene solvent, in both **1a** and **1aTHF-1** species, the absorption peak is red-shifted by 10 nm with respect to the gas phase. Likewise, the major Soret peak for the **1a** tautomer is similar in all functionals used and ranges from 373 to 397 nm, in the gas phase and in the **1aTHF-1** structure the peak is red-shifted by about 10 nm. In toluene solvent, for both **1a** and **1aTHF-1** species the peak is red-shifted by about 20 nm.

The **1aTHF-1** and **1aTHF-2** species differ in the type of interaction of THF with the **1a** tautomer. In the **1aTHF-1** structure, the THF is perpendicular to **1a**, while in the **1aTHF-2** structure the THF ring is parallel to the ring of the NCP. In **1aTHF-1**, the presence of THF deforms the **1a** isomer, see Figure 1, and slightly deforms its frontier MOs; see Supporting Information. This deformation may result in a quasi-Jahn–Teller effect (as mentioned above the frontier MOs strikingly resemble those of the  $D_{4h}$  tetraphenylporphyrin) depressing the H-1 and raising the H orbital energy, thus reducing the H–L gap and leading to a red shift. Thus, in the **1aTHF-1** structure, the lowest-energy Q peak is significantly red-shifted, up to 40 nm, while the

Soret peak is red-shifted up to 10 nm in the gas phase or in toluene solvent with respect to the **1aTHF-2** structure. In **1aTHF-2**, the corresponding peaks are practically not shifted with respect to the peaks of **1a**, because the interaction between THF and **1a** is smaller and the relative energy of the four frontier orbitals is practically the same in both **1a** and **1aTHF-2**. Thus, different interactions cause different shifts in some absorption peaks. Finally, the corresponding Q and Soret peaks in the **1aLi-1** and **1aLi-2** species are blue-shifted by about 20 nm and red-shifted by about 10 nm, respectively, with respect to the corresponding peaks of the **1a** tautomer, see Figure 4 and Table 2S of the Supporting Information.

**1b and 2 NCPs.** For the lowest-energy Q peak and the major absorption peak of the Soret band, of the **1b** tautomer, and the **2** NCPs, the three functionals present large deviations of the  $\lambda$  values of about 100 and 40 nm, respectively; see Table 6. However, for the complexes which include the **1b** or **2** species the corresponding deviations are smaller, up to 70 and 40 nm, respectively. The CAM-B3LYP and M06-2X functionals present similar absorption peaks, while the B3LYP functional predicts red-shifted values with respect to the other two functionals.

The insertion of Li in the **1b** tautomer and in the **2** porphyrin results in red shifts ranging from 60 to 100 nm for the Q peak depending on the functional used and 15 nm for the Soret peak

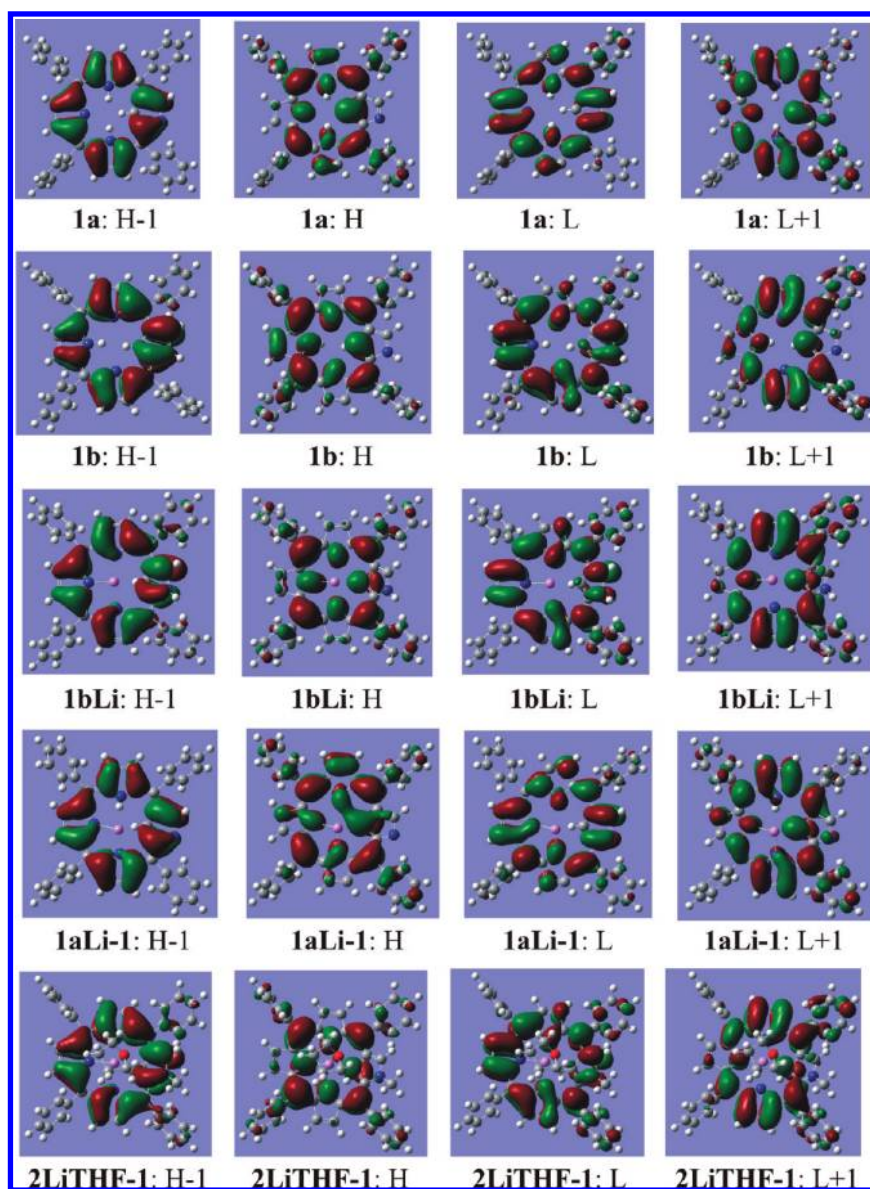


Figure 5. Plots of the M06-2X frontier canonical molecular orbitals for the **1a**, **1b**, **1bLi**, **1aLi-1**, and **2LiTHF-1** species.

using all three functionals. These red shifts in the lowest-energy Q peaks are expected because Li interacts with more N atoms than the hydrogen atom which binds only to one N atom, Li is slightly more positive and less electronegative than H, and as a result the HOMO–LUMO difference becomes smaller when the hydrogen is replaced by the Li atom. That causes red shifts in the lowest-energy Q peak. The additional interaction of the THF with the Li-NCP results in a further decrease in the energy difference between H and L and a further red shift in the lowest-energy Q peak. In the toluene solvent, the interaction of the **1bLiTHF** and **2LiTHF** with the solvent leads to another red shift of 10–15 nm with respect to the gas phase, in all cases. The relative energies of the four frontier orbitals are given in the Supporting Information. Finally, the spectra of the different **1bTHF** structures, resulting from the interaction of the **1b** with THF, are given in the Supporting Information.

Sripothongnak and Ziegler<sup>8</sup> measured the UV–vis spectra of N-confused tetraphenylporphyrin in anhydrous 5% THF in toluene and its lithium complex in the same solvent. Their structures corresponds to our **1aTHF-1** and **1bLiTHF-1** structures in toluene

solvent. The experimental lowest-energy Q and Soret peaks appear at 443 and about 710 nm for the NCP and at 468 and 739 nm for the Li complex, respectively. Our calculated values for the **1aTHF-1** structure are 425 and 689 nm using the B3LYP functional and 403 and 663 nm using the M06-2X or CAM-B3LYP functional; see Table 6 and Figure 4. For the **1bLiTHF-1** structure, the peaks are at 442 and 765 nm using the B3LYP functional and 407 and 692 nm using the M06-2X or CAM-B3LYP functional; see Table 6. It might be noted that in our calculations we have one THF molecule next to the **1a** tautomer of the NCP and to the lithium complex of the NCP, as opposed to the experimental spectra where each complex is surrounded by 6 THF molecules.<sup>8</sup> Thus, the lower THF concentration in the calculation might justify the blue shifts in the calculated spectra.

It seems that TD-B3LYP calculations yield  $\lambda$  values that are in better agreement with the above experimental values than the TD-CAM-B3LYP or TD-M06-2X techniques. The deviations of the B3LYP  $\lambda$  values from the experimental ones range from 26 to –26 nm, while the deviations of the M06-2X  $\lambda$  values range from

40 to 61 nm. Vibronic coupling that has not been taken into account in our calculations can result in peak shifts.<sup>30–32</sup> The largest discrepancy between experiment and the M06-2X calculations is observed for the major Soret peak and corresponds to a blue shift of 0.40 eV and the smallest one to the lowest-energy Q peak, namely, 0.11 eV. The CAM-B3LYP functional presents similar discrepancies with M06-2X. Other TDDFT and ab initio calculations on normal porphyrins derivatives can also present for some peaks similar discrepancies between experiment and calculations.<sup>10,33</sup> Moreover, it has been shown that increasing the size of the basis sets only slightly affect the absorption spectra on normal porphyrins.<sup>33</sup> Peaks calculated by TD-B3LYP show the smallest shifts which range from 0.06 to 0.16 eV. Shifts up to 0.2 eV are considered as showing very good agreement between experimental and TDDFT calculations.<sup>33</sup> Finally, the TD-CAM-B3LYP relative intensity of the lowest-energy Q peak and the major Soret peak is calculated to be 10 and 6 for the **1a**THF-**1** and **1b**LiTHF-**1** structures, while the B3LYP values are 8 and 5. The corresponding experimental relative intensities are 11 and 7, in very good agreement with the TD-CAM-B3LYP values.

The N, L, and M bands are located at ~350, 300–330, and ~250 nm using the B3LYP functional; see Figures 4 and 1S–6S of the Supporting Information. The CAM-B3LYP and M06-2X peaks are blue-shifted 20–30 nm with respect to the B3LYP values.

#### IV. SUMMARY AND CONCLUSIONS

Recently, the lithium complexes of the N-confused tetraphenylporphyrin and the externally N-methylated N-confused tetraphenylporphyrin were synthesized by Sripithongnak and Ziegler.<sup>8</sup> The motivation of the present study was the explanation of the unusual coordination environment that is adopted by the Li atom<sup>8</sup> and to see how the Li binding affects the Q and the Soret band. Thus, we studied the electronic and geometric structures of the two tautomers of the N-confused tetraphenylporphyrin, the externally N-methylated N-confused tetraphenylporphyrin, as well as lithium complexes of the two porphyrins in the presence or absence of tetrahydrofuran (THF) in the gas phase and in toluene solvent. All calculations have been carried out employing the DFT and TDDFT methods, using the B3LYP, CAM-B3LYP, and M06-2X functionals in conjunction with the 6-31G(d,p) basis set. The theoretical work extends over a wider type of structures for the complexes and includes reaction energies, enthalpies, reaction paths, and absorption spectra. While it confirms the experimental conclusions for the most part, a different interpretation is provided regarding the type of bonding involved in the complexes. A summary of our main results follows.

The M06-2X functional has been found to be more suitable for the calculation of the reaction energies and the geometries. However, all three functionals predict similar geometries, in agreement with the crystallographic data where they are available. Moreover, they yield the same population analyses.

The reaction energy for the insertion of lithium into NCP and 21-N-methylated N-confused porphyrin, namely,  $\text{NCP} + \text{LiN}(\text{Si}(\text{Me})_3)_2 \rightarrow \text{Li-NCP} + \text{HN}(\text{Si}(\text{Me})_3)_2$ , has been calculated to  $-67.6(-55.4)$  and  $-72.4(-59.3)$  kcal/mol in the gas phase (in toluene solvent) in the presence of THF. The corresponding enthalpies of above reaction at 1 atm and 298.15 K are  $-65.2(-54.1)$  and  $-70.2(-58.1)$  kcal/mol. Finally, the reaction energy for the N-confused porphyrin in the absence of THF is  $-47.7(-37.3)$  kcal/mol.

In agreement with the experiment the Li atom is found to adopt an unusual coordination environment. The reason is that,

unlike a typical tetrahedral  $\text{Li}^+$  cation, this Li has a fractional positive charge of about  $+0.5 e^-$ , forms a  $\sigma$  bond with one N, interacts with the remaining two N atoms, and is located in the right place to form an agostic-like interaction with a core C–H bond. In the presence of the THF, the Li atom interacts via its empty p orbital which is perpendicular to the macrocycle of the NCP with the O atom of the THF, which is also perpendicular to the macrocycle, in agreement with the experimental data.

Absorption spectra, based on about 50 excited electronic states of the complexes, have been determined at the optimized ground state geometry in order to calculate the Q, B, N, L, and M bands. UV–vis spectra of the conformers are similar using either M06-2X or CAM-B3LYP functional, while the corresponding B3LYP peaks are shifted to smaller energies, which are in better agreement with experimental values. The largest discrepancy between experiment and the calculations (M06-2X) is observed for the major Soret peak and corresponds to a blue shift of 0.4 eV, while the B3LYP peak shifts range from 0.06 to 0.16 eV. For all complexes which include the **1a** NCP, the general shape of the UV–vis spectra is the same. Likewise, the same stands for all structures including the **1b** and **2** NCPs. Moreover, differences in the interactions of the conformers, result in differences in their calculated spectra. It is found that the general 4 electron–4 orbital model often employed for the description of the excited states of porphyrins is applicable here too, for the description of the main spectral features of the complexes of Li with NCP. Finally, as the number of the interactions in a species increases, i.e., by replacing H with Li and adding THF or solvent, the lowest-energy Q peak is more red-shifted.

#### ■ ASSOCIATED CONTENT

**S** Supporting Information. Geometries, Mulliken charges, relative energies of H-1, H, L, and L+1 molecular orbitals, excitation energies, absorption selected peaks, oscillator strengths, main excitations and their coefficient contributing to the excited state of the calculated species in the gas phase and in toluene solvent at the B3LYP, CAM-B3LYP, and M06-2X/6-31G(d,p) levels of theory are given in Tables 1S–5S. The absorption spectra of the calculated species in the gas phase and in toluene solvent calculated at the B3LYP, CAM-B3LYP, and M06-2X/6-31G(d,p) level of theory are depicted in Figures 1S–6S. Molecular orbitals plots are depicted in Figure 7S. This material is available free of charge via the Internet at <http://pubs.acs.org>.

#### ■ AUTHOR INFORMATION

##### Corresponding Author

\*Fax: +30-210-7273-794. Phone: +30-210-7273-813. E-mail: dtzeli@eie.gr.

#### ■ ACKNOWLEDGMENT

Financial support from the EU FP7, Capacities Program, NANOHOST project (GA 201729), and the NATO Grant CBP.MD.CLG.983711 is acknowledged. We also thank the reviewers and the referee for helping improve this paper through their detailed comments.

#### ■ REFERENCES

(1) Furuta, H.; Asano, T.; Ogawa, T. *J. Am. Chem. Soc.* **1994**, *116*, 767–768.

- (2) Chmielewski, P. J.; Latos-Grazynski, L.; Rachlewicz, K.; Glowiak, T. *Angew. Chem., Int. Ed. Engl.* **1994**, *33*, 779–781.
- (3) (a) Furuta, H.; Maeda, H.; Osuka, A. *Chem. Commun.* **2002**, 1795–1804. (b) Pushpan, S. K.; Chandrashekar, T. *Pure Appl. Chem.* **2002**, *74*, 2045–2056. (c) Srinivasan, A.; Furuta, H. *Acc. Chem. Res.* **2005**, *38*, 10–20. (d) Çetin, A.; Durfee, W. S.; Ziegler, C. J. *Inorg. Chem.* **2007**, *46*, 6239–6241.
- (4) (a) Maeda, H.; Furuta, H. *J. Porphyr. Phthalocyanines* **2004**, *8*, 67–76. (b) Maeda, H.; Furuta, H. *Pure Appl. Chem.* **2006**, *78*, 29–44.
- (5) Toganoh, M.; Harada, N.; Morimoto, T.; Furuta, H. *Chem.—Eur. J.* **2007**, *13*, 2257–2265 and references therein.
- (6) (a) Harvey, J. D.; Ziegler, C. J. *Coord. Chem. Rev.* **2003**, *247*, 1–19. (b) Ghosh, A. *Angew. Chem., Int. Ed.* **2004**, *43*, 1918–1933. (c) Chmielewski, P. J.; Latos-Grazynski, L. *Coord. Chem. Rev.* **2005**, *249*, 2510–2533. (d) Jiang, H.-W.; Chen, Q.-Y.; Xiao, J.-C.; Gu, Y.-C. *Chem. Commun.* **2008**, 5435–5437.
- (7) Yeguas, V.; Cárdenas-Jirón, G. I.; Menéndez, M. I.; López, R. *J. Math. Chem.* **2010**, *48*, 137–144 and references therein.
- (8) Sripothongnak, S.; Ziegler, C. J. *Inorg. Chem.* **2010**, *49*, 5789–5791.
- (9) (a) Gebauer, A.; Dawson, D. Y.; Arnold, J. J. *Chem. Soc., Dalton Trans.* **2000**, 111–112. (b) Xu, L.-C.; Li, Z.-Y.; He, T.-J.; Liu, F.-C.; Chen, D.-M. *Chem. Phys.* **2004**, *305*, 165–174. (c) Cissell, J. A.; Vaid, T. P.; Yap, G. P. A. *Org. Lett.* **2006**, *8*, 2401–2404. (d) van Kampen, J. J. A.; Luider, T. M.; Ruttink, P. J. A.; Burgers, P. C. J. *Mass Spectrosc.* **2009**, *44*, 1556–1564. (e) De Luca, G.; Romeo, A.; Scolaro, L. M.; Ricciardi, G.; Rosa, A. *Inorg. Chem.* **2009**, *48*, 8493–8507.
- (10) Vyas, S.; Hadad, C. M.; Modarelli, D. A. *J. Phys. Chem. A* **2008**, *112*, 6533–6549.
- (11) Tzeli, D.; Papakondylis, A.; Mavridis, A. *J. Phys. Chem. A* **1998**, *102*, 2223–2230.
- (12) (a) Becke, D. J. *Chem. Phys.* **1993**, *98*, 1372–1377. (b) Lee, C.; Yang, W.; Parr, R. G. *Phys. Rev. B* **1988**, *37*, 785–789.
- (13) (a) Yanai, T.; Tew, D.; Handy, N. *Chem. Phys. Lett.* **2004**, *393*, 51–57. (b) Tawada, Y.; Tsuneda, T.; Yanagisawa, S.; Yanai, T.; Hirao, K. *J. Chem. Phys.* **2004**, *120*, 8425–8433. (c) Peach, M. J. G.; Benfield, P.; Helgaker, T.; Tozer, D. J. *J. Chem. Phys.* **2008**, *128*, 044118(1–8). (d) Stein, T.; Kronik, L.; Baer, R. *J. Am. Chem. Soc.* **2009**, *131*, 2818–2820.
- (14) (a) Zhao, Y.; Truhlar, D. *Theor. Chem. Acc.* **2008**, *120*, 215–241. (b) Zhao, Y.; Truhlar, D. *Acc. Chem. Res.* **2008**, *41*, 157–167.
- (15) Curtiss, L. A.; McGrath, M. P.; Blaudeau, J.-P.; Davis, N. E.; Binning, R. C., Jr.; Radom, L. *J. Chem. Phys.* **1995**, *103*, 6104–6113.
- (16) Miertuš, S.; Scrocco, E.; Tomasi, J. *Chem. Phys.* **1981**, *55*, 117–129.
- (17) (a) Cossi, M.; Scalmani, G.; Rega, N.; Barone, V. *J. Chem. Phys.* **2002**, *117*, 43–54. (b) Tomasi, J.; Mennucci, B.; Cammi, R. *Chem. Rev.* **2005**, *105*, 2999–3093. (c) Pedone, A.; Bloino, J.; Monti, S.; Prampolini, G.; Barone, V. *Phys. Chem. Chem. Phys.* **2010**, *12*, 1000–1006.
- (18) Marques, M. A. L.; Gross, E. K. U. *Annu. Rev. Phys. Chem.* **2004**, *55*, 427–455.
- (19) Harvey, P. D. *The Porphyrin Handbook*, Kadish, K. M.; Smith, K. M.; Guillard, R., Eds.; Academic Press: San Diego, 2003.
- (20) Boys, S. F.; Bernardi, F. *Mol. Phys.* **1970**, *19*, 553–566.
- (21) (a) Jeziorski, B.; Moszynski, R.; Szalewicz, K. *Chem. Rev.* **1994**, *94*, 1887–1930. (b) Tzeli, D.; Mavridis, A.; Xantheas, S. S. *J. Phys. Chem. A* **2002**, *106*, 11327–11337.
- (22) Frisch, M. J.; Trucks, G. W.; Schlegel, H. B.; Scuseria, G. E.; Robb, M. A.; Cheeseman, J. R.; Scalmani, G.; Barone, V.; Mennucci, B.; Petersson, G. A.; Nakatsuji, H.; Caricato, M.; Li, X.; Hratchian, H. P.; Izmaylov, A. F.; Bloino, J.; Zheng, G.; Sonnenberg, J. L.; Hada, M.; Ehara, M.; Toyota, K.; Fukuda, R.; Hasegawa, J.; Ishida, M.; Nakajima, T.; Honda, Y.; Kitao, O.; Nakai, H.; Vreven, T.; Montgomery, Jr., J. A.; Peralta, J. E.; Ogliaro, F.; Bearpark, M.; Heyd, J. J.; Brothers, E.; Kudin, K. N.; Staroverov, V. N.; Kobayashi, R.; Normand, J.; Raghavachari, K.; Rendell, A.; Burant, J. C.; Iyengar, S. S.; Tomasi, J.; Cossi, M.; Rega, N.; Millam, N. J.; Klene, M.; Knox, J. E.; Cross, J. B.; Bakken, V.; Adamo, C.; Jaramillo, J.; Gomperts, R.; Stratmann, R. E.; Yazyev, O.; Austin, A. J.; Cammi, R.; Pomelli, C.; Ochterski, J. W.; Martin, R. L.; Morokuma, K.; Zakrzewski, V. G.; Voth, G. A.; Salvador, P.; Dannenberg, J. J.; Dapprich, S.; Daniels, A. D.; Farkas, O.; Foresman, J. B.; Ortiz, J. V.; Cioslowski, J.; Fox, D. J. *Gaussian 09*, revision A.1; Gaussian, Inc., Wallingford CT, 2009.
- (23) (a) Furuta, H.; Ishizuka, T.; Osuka, A.; Dejima, H.; Nakagawa, H.; Ishikawa, Y. *J. Am. Chem. Soc.* **2001**, *123*, 6207–6208. (b) Belair, J. P.; Ziegler, C. J.; Rajesh, C. S.; Modarelli, D. A. *J. Phys. Chem. A* **2002**, *106*, 6445–6451.
- (24) Molnar, L. F.; He, X.; Wang, B.; Merz, K. M., Jr. *J. Chem. Phys.* **2009**, *131*, 065102(1–16).
- (25) Bickelhaupt, F.; Hommes, N.; Guerra, C.; Baerends, E. *Organometallics* **1996**, *15*, 2923–2931. Baerends, E. J.; Gritsenko, O. V. *J. Phys. Chem. A* **1997**, *101*, 5383–5403. Ishikawa, S.; Madjarova, G.; Yamabe, T. *J. Phys. Chem. B* **2001**, *105*, 11986–11993.
- (26) Maseras, F.; Morokuma, K. *Chem. Phys. Lett.* **1992**, *195*, 500–504.
- (27) Guerra, C. F.; Handgraaf, J.-W.; Baerends, E. J.; Bickelhaupt, F. M. *J. Comput. Chem.* **2004**, *25*, 189–210.
- (28) (a) Petsalakis, I. D.; Tagmatarchis, N.; Theodorakopoulos, G. *J. Phys. Chem. C* **2007**, *111*, 14139–14149. (b) Petsalakis, I. D.; Theodorakopoulos, G. *Chem. Phys. Lett.* **2008**, *466*, 189–196. (c) Petsalakis, I. D.; Tzeli, D.; Kerkines, I. S. K.; Theodorakopoulos, G. *Comput. Theoret. Chem.* **2011**, *965*, 168–175.
- (29) Tzeli, D.; Petsalakis, I. D.; Theodorakopoulos, G. *Phys. Chem. Chem. Phys.* **2011**, *13*, 11965–11975.
- (30) Stradomska, A.; Knoester, J. *J. Chem. Phys.* **2010**, *133*, 094701(1–10).
- (31) Andrade, S. M.; Teixeira, R.; Costa, S. M. B.; Sobral, A. J. F. N. *Biophys. Chem.* **2008**, *133*, 1–10.
- (32) Ribó, J. M.; Bofill, J. M.; Crusats, J.; Rubires, R. *Chem.—Eur. J.* **2001**, *7*, 2733–2737.
- (33) Improta, R.; Ferrante, C.; Bozio, R.; Barone, V. *Phys. Chem. Chem. Phys.* **2009**, *11*, 4664–4673.
- (34) (a) Gouterman, M. *J. Mol. Spectrosc.* **1961**, *6*, 138–163. (b) Edwards, L.; Dolphin, D. H.; Gouterman, M.; Asler, A. D. *J. Mol. Spectrosc.* **1971**, *38*, 16–32.